INVESTIGATION OF MICRO SPIRAL WAVES AT CELLULAR LEVEL USING A MICROELECTRODE ARRAYS TECHNOLOGY

Sabir Jacquir, Stéphane Binczak, Binbin Xu, Gabriel Laurent, David Vandroux, Pierre Athias, Jean-Marie Bilbault

INVESTIGATION OF MICRO SPIRAL WAVES AT CELLULAR LEVEL USING A MICROELECTRODE ARRAYS TECHNOLOGY

[1,*]S. Jacquir,[1]S. Binczak,[1]B. Xu,[1]G. Laurent,[2]D. Vandroux,[3]P. Athias,[1]J.M. Bilbault

[1]Laboratoire LE2I, UMR CNRS 5158, Université de Bourgogne, Dijon, France.

[2]NVH Medicinal, Dijon, France.

[3]Institut de Recherche Cardiovasculaire, CHU Le Bocage, Dijon, France.

[*]sjacquir@u-bourgogne.fr

February 4, 2010

Abstract

During cardiac arrhythmia, functional reentries may take the form of spiral waves. The purpose of this study was to induce spiral waves by an electrical stimulation of cultured neonatal

rat cardiomyocytes using a microelectrode arrays technology. In basal conditions, cardiac muscle cells in monolayer culture displayed a planar wavefront propagation. External electrical impulse trains induced severe arrhythmia and spiral waves appeared. This in vitro generation of spiral wave opens a new way to test the anti-arrhythmic drugs and for strategies at microscopically scale.

Keywords: *Spiral wave; MicroElectrode Array (MEA) Technology; Cardiac cells; Fibrillation.*

1 Introduction

Despite abundant research, the mechanisms of cardiac arrhythmias are still poorly understood. Many studies of cardiac arrhythmia focused on the spatiotemporal propagation of the electrical waves throughout the myocardium [Wang et al, 2003; Winfree, 1994; Agladze et al, 1994; Gray et al, 1995, 1997; Everett et al, 2006]. In particular, the formation of spiral waves (SW) has been suspected to be responsible for fibrillation phenomena. Experimental evidence that functional reentrant SW are present in cardiac tissue was given by some previous reports [Allessie et al, 1973; Davidenko et al, 1990, 1992; Pertsov et al, 1993]. Recent in vitro studies have suggested that maintenance of arrhythmia may depend on the periodic activity of a small number of rotors or spiral waves [Jalife, 2003; Laurent et al, 2008a,b]. These SW activate the tissue substrate (atria or ventricles) at high frequencies and result in fibrillation behavior. However, the analysis and understanding of the SW appearance are very difficult for several reasons. The heart is anatomically complex, composed of different tissues

and functionally instable. In particular, it is hard to maintain the heart in a stationary state (anatomical position, stable rhythm) for a long period. The whole heart imaging techniques based on the use of fluorescent dyes for the visualization of the cardiac activation waves are quite invasive, do not permit long duration observation periods and can affect tissue cells and functions. In addition, applied to heart cell cultures, the observation of the electrical activation spread with voltage-sensitive dyes is suspected to be rather cytotoxic and limited by its poor spatial resolution [Fast & Kleber, 1995; Lim et al, 2006; Koura et al, 2002].

Multi-electrodes investigation is an alternative method that is devoid of the dye toxicity, but the drawback of this approach is limited by its rather rough spatial resolution in the case of the whole heart. To overcome these in vivo heart studies limitations, primary cultures of cardiac muscle cells have been developed [Athias et al, 2006]. This cellular preparation gives access to repeated, long term recording duration periods and to easy comparison of experimental data with those of analytical and/or computational studies. Monolayer cultures of cardiac myocytes (CM) represent thus a promising experimental model for the study of cardiac electrophysiology and arrhythmogenesis. It can be used to study the elementary phenomenon at the basis of the activation spread within cardiac muscle and at the origin of the lethal rhythm troubles, such as myocardial fibrillation, reentry with a particular interest with reentrant (spiral) waves. Extracellular recordings of electrical activity with substrate-integrated microelectrode arrays (MEA) enable non-invasive and non toxic long-term monitoring of contractile multicellular cardiac preparations [Pillekamp et al, 2006; Stett et al, 2003; Banach et al,

2003; Hescheler et al, 2004]. Moreover, the MEA technology has a better spatial resolution than the fluorescence mapping procedure and is a less invasive technique than the conventional electrophysiological methods, i.e., intracellular or patch clamp technique.

In our precedent works, we have validated the use of the MEA technology for the study of the impulse propagation pattern in cardiac cell culture in the basal conditions [Athias et al, 2007]. The purpose of the present study was to explore the basal mechanisms of cardiac arrhythmogenesis, and the possible occurrence of elementary SW at the cellular scale using neonatal rat cardiomyocytes in monolayer culture on microelectrode arrays device (MEA). Our preliminary results showed that it was possible to generate arrhythmias and SW by submitting the cell monolayer to external electrical impulse trains [Laurent et al, 2008c; Athias et al, 2009; Jacquir et al, 2009a,b], in agreement with previous reports suggesting that rapid pacing may be able to alter cardiac conduction [Kondratyev et al, 2007]. Studying SW at a cellular scale may lead to a better understanding of the way by which these microscopic rotors may be able to evolute and to stabilize in the myocardial tissue substrate. It also may be useful for the development of innovative approaches for prevention, diagnosis, and treatment of cardiac arrhythmias.

This paper is organized as follows: Section (2) describes the CM culture preparation, the multielectrode array recording procedure and the stimulus generator device. Section (3) presents the experimental results and their analysis by using nonlinear dynamical system techniques such as bifurcation diagram and Poincaré maps [Garfinkel et al, 1997; Beuter et al, 2003]. A discussion and conclusion

section finishes this paper.

2 Materials and Methods

2.1 Cardiomyocyte culture preparation

One of the major requirement of the cell culture techniques is that all stages of the preparation and the growth must be done in strictly sterile conditions. Neonatal myocytes were prepared from 1 to 4 days-old Wistar rats by trypsin-based enzymatic dispersion as described previously [Athias et al, 1987; Grynberg , 1986]. The cell suspension was preplated twice in Ham's $F10$ medium supplemented with fetal calf serum (FCS) and penicillin/streptomycin (100 U/ml) in order to increase cardiomyocyte (CM) proportion. Cardiomyocyte-rich cultures ($> 90\%$) were seeded at a final density of 10^5 cells per cm^2 in supplemented Ham's $F10$ medium. Cultures were incubated in a humidified incubator (95% air, 5% CO_2 at 37° C) and were used after 4-5 days of growth, a step at which confluent and spontaneously beating cell monolayers were obtained. Figure 1 shows a picture of an isolated CM obtained according to this cell culture procedure.

2.2 Multielectrode array recordings

CM were grown on multi-electrode arrays allowing non-invasive synchronous multifocal field potential (FP) recordings. MEA consists of 60 substrate-integrated microelectrode arrays (8×8 matrix, 30

μm electrode diameter, 200 μm inter-electrode distance). Figures 2(a,b,c) show the MEA supporting a cardiac cell monolayer culture used in our experiments. The MEAs give access to the cellular electrocardiogram (ECG), determined by the transmembraneous electrical changes during periodic action potentials in the cardiac muscle cell in contact with each surface microelectrode. MEA allows thus the long term, non-traumatic recording from individual and together with the simultaneous, parallel monitoring of tens of cells in the same MEA dish in an easily controlled environment. This approach permits to evaluate the multifactorial influence - including signal propagation and spatial inhomogeneity - of experimental factors such as drugs and physicochemical stress. The complete experimental setup is shown in Figure 3. The 60 signals originating from the MEA are acquired with a maximum sampling rate of 50 $kHz/channel$ with a 12 bits resolution. The amplification device containing the MEA ((A) on Fig.3) is placed inside a Faraday enclosure ((B) on Fig.3) to reduce electrical noise and interferences. A separate device ((C) on Fig.3) controls and maintains temperature at 37° C. Data are acquired and analyzed with a customized platform programmed with LABVIEW (National Instruments) and MATLAB (Mathworks) in order to provide two-dimensional electrophysiological maps derived from these multisite FP recordings (Computer (D) on Fig. 3).

3 Results

Each of the 60 microelectrodes embedded in the bottom of MEA dishes allow the long-term recordings of the extracellular electrical activity, that is, field potentials (FP), which reflects the external electrical signal resulting from CM membrane potential changes during the course of each action potential. Recorded data are classified either as normal or as abnormal signals using the continuous wavelet transform tools [Jacquir et al, 2009c]. Figure 4(a) displays an example of data resulting from this selection routine.

3.1 Propagation of field potential in basal conditions

In first, field potential signals are recorded on basal conditions, which means that cells are not stressed and are in nutritive bath. In this case, the analysis of the spontaneous FP spikes (Fig. 4(b)) indicates that the mean frequency in the case of data presented in Fig. 4(a) corresponds to about 90 beats per minute. In addition, a moderate variability of the FP frequency between electrodes and between each period is observed, which may be due to a remodeling phenomenon of gap junctions [Rohr, 2004], spontaneous fluctuations of the ionic channel function, or random changes in the propagation path. This last hypothesis appears consistent with previous propagation data from intracellular recordings of the action potentials [Athias et al, 2007]. Observing the distribution of the mean period of the FP (Fig. 5), one can conclude that the MEA system is relatively stable and robust.

The local activation time (LAT) corresponds to the FP spike appearance on each electrode in a temporal scale (see an example of FP time serie on Fig. 4(b)). Thus, the LAT is determined for each FP spike for each electrode. Then a ranking is established by ordering FP spike appearance on the 60 electrodes between each period, which leads to an activation map and enables to display the propagation path followed by the FP spikes during each period. The consecutive period to period activation maps corresponding to the signals shown in Fig. 4(a) are reported in Fig. 6. The number inserted in each colored panel corresponds to the rank of the FP spike activation (refer to Fig. 6a). From the global view of these activation maps, it can be concluded that the FP spikes propagate following a quasi-straight path, materialized by the white arrows in Figs. 6(a to h). However, the examination of the individual rank of order of FP spike activation reveals that the FP spike propagation pathway fluctuates at each period. This might mean that FP cell-to-cell propagation is not trivial, despite the fact that the overall propagation throughout the multicellular sheet is planar.

These field potential mappings confirm thus that the cultured cardiomyocytes display highly synchronous electrical activity and that the FP-derived parameters remain stable and homogeneous, as already described for conventional endocellular recordings [Tissier , 2002].

3.2 Field potential analysis in arrhythmia after electrical stimulation

The electrical stimulation of cultured cell stimulation requires electrical pulses with very low amplitude and a high signal to noise ratio. The stimulus generator delivers high quality pulse amplitude ranging between in 10 μV to 1 mV, with accurately adjustable frequency and duty cycle. In this case, cardiomyocytes are electrically stressed by external electrical shocks consisting in a stimulation impulse trains (burst of 200 μV at 100 Hz during 5 minutes) which are applied at one microelectrode M_1 located at the edge of the MEA (see Fig. 2(a)). The stimulation frequency is chosen purposely higher than the FP spike frequency because in order to disrupt the CM activity. This stimulation protocol causes alterations in CM electrical activity, that is depicted by the recording of irregular and disordered FP. The evolution of the FP period vs. time is given in Fig. 7 expressing a bifurcation scenario. At first, the cells display a regular rhythm corresponding to basal conditions with a FP spikes period $T = 0.667$ s (cf sec.(3.1)). The stimulation is then applied at the microelectrode M_1 at $t = 0$ and during 5 minutes. The cells become unstable and express a chaotic state one hour after stimulation, as illustrated by event (A) on Fig. 7. Thereafter, a period doubling phenomenon is observed (event (B) for $t = 3h$ on Fig. 7), then a transitory reversal to a stable state takes place (event (C) at $t = 4h$ on Fig. 7), and finally a reappraisal of an unstable and disordered state can be observed.

It is well known that any system which makes a transition from order to disorder through the period-doubling phase, whatever the exact functional nature of these systems, displays common properties. These properties found in dynamic systems can be investigated using a Poincaré map tool. In contrast

to random behavior, deterministic behavior means that the present state of a system is determined by its previous states. A simple test for such a relationship is a Poincaré plot, in which each successive value of a system variable is plotted against its previous value. For a purely random system, the distribution of points on a Poincaré plot is formless, whereas for a system with significant nonrandom elements, the points often form a distinct structure. Therefore, We constructed Poincaré plots of interactivation intervals (FP period P_{n+1} vs. P_n). Before stimulation, in basal conditions (data of Fig. 4(a)), only stable fixed points are found in Poincaré map for each individual electrode, the number n of periods being the same for all electrodes. Data points (cross symbol in Fig. 8) can be considered as stable attractors and describe a periodic cycle in the Poincaré section. In this case, the FP frequency is regular and stable in the considered period of time.

During atrial, ventricular tachycardia (or bradycardia), interactivation intervals (FP periods) are nearly constant, but during fibrillation they become highly irregular, as shown in Fig. 7. Analyzing the time series of the FP at event (A), that is one hour after the stimulation, the arrhythmic periods indicate that the rate is irregular as compared to basal conditions (at $t = 0$ on Fig. 7). In this electrical shock-induced chaotic state (Fig. 9(a)), the number n of periods is different from one electrode to another and the number of attractors is different for each electrode. Attractors are not stable and move around the bissector (Fig. 9(b)). For the following events, the attractors move between two positions along the bissector which correspond to the period doubling phase (see Figs. 10(b) for event (B) of Fig. 7). Note that this period doubling is a localized phenomenon in the CM culture. Four hours after stimu-

lation, the CM spontaneous rhythm became normal again and stable (see event (C) in the bifurcation diagram (Fig. 7), the time series and the Poincaré map corresponding to this event are depicted in Fig. 11). However, CM did not stay in this state since they bifurcate afterwards again to a chaotic state (see $t = 4.5h$, $t = 5h$... in Fig. 7). These changes might mean that the cells are in a state of a sustained arrhythmia, but transitory switchs between the basal rhythm and unstable rhythms which may occur. Our results are in accordance with [Garfinkel et al, 1997], where the authors suggested that the fibrillation is a form of spatiotemporal chaos arising via a quasiperiodic transition. Our results suggest that this mechanism is present at a microscopic scale. The idea that multifrequency quasiperiodicity is inherently unstable and will degenerate into chaos was first suggested by Ruelle and Takens [Ruelle & Takens, 1971]. The quasiperiodic scenario explains the origin of the ring lake structures seen in the Poincaré plots. The qualitative description of the functional behavior of our experimental model depicted by the Poincaré maps is confirmed using the activation maps during a period of regular rhythm and during an arrhythmic state. Activation mapping during regular rhythm reveals a planar propagation wavefront (see Fig. 6). In contrast, the activation maps reveal the occurrence of relatively stable counter-rotating micro spiral waves during a sustained induced arrhythmia episode induced by external electrical stimulation. For the visualization, a real time movie is realized and some snapshots corresponding to the evolution of one of the displayed SW at different moments are given in Fig. 12. This is an example of SW obtained from the data depicted on Fig. 9. In this case, an average of 3 ± 1 SW is observed within the surface explored by the microelectrodes array, that is 2.5 mm^2; due to their

smallness, they are rather micro SW, and they could be a sign of a chaotic state of the system. These rotation waves appear to be random and could be submitted to period-to-period fluctuations. They are able to translocate, since they can move within or away the recording area. They have a mean radius of 400 $\pm$ 100 μm and a mean angular velocity of 300 $\pm$ 50 rotations per minute. Unstable reentrant and colliding wavefronts are also observed during an arrhythmic episode.

4 Discussion and conclusion

Concerning the origin of the myocardial fibrillation phenomena, and in opposition to the multiple wavelets theory [Moe et al, 1964], the SW model implies the existence of localized and stable high frequency areas. Primary cultures of cardiac cells on MEA constitute an emerging experimental model for studying cardiac electrophysiology and arrhythmia at the cellular scale and in highly controllable conditions. In addition, this model system permits to develop electrical shock-induced simulation of cardiac arrhythmia and the experimental data collected with this model may be compared with those of analytical and/or computational studies. Extracellular recordings of electrical activity with substrate-integrated MEA enable indeed true non-cytotoxic and non-invasive long-duration monitoring of spontaneously contracting sheets of cultured cardiac muscle cells. This method features a better spatial and time resolution than the optical mapping techniques and is much less hurtful than the conventional endocellular electrophysiological technique. The present data from in vitro MEA

exploration confirm that monolayer cultures of cardiac muscle cells beat at very stable and regular rate and that this spontaneous electromechanical activity propagates along linear pathways throughout the cellular sheet. Laterally-imposed low-voltage electrical impulse trains cause highly disordered electrical activity and severe irregularities of the endogenous rhythm and of the propagation process, mimicking myocardial fibrillation. During these experimentally-induced arrhythmic episodes, the unprecedented observation of micro SW has been realized. They can be accurately quantified in terms of size, rotational speed, duration and displacement. These data could be related, for mechanistic and understanding purpose, to the other FP (cellular ECG) parameters, i.e. duration, rising and falling deflection speed, deflection polarity and local propagation speed. This novel in vitro model of experimentally-induced sustained arrhythmias, mimicking fibrillation patterns, may be helpful in the comprehension of cardiac arrhythmogenesis in clinical situations and may be useful to provide an experimental basis of new treatments and prevention strategies. Therefore, although it should be take into account the limitations of the model, related to its simplified 2D geometry and the absence of neural and hormonal influences, the MEA technique applied to monolayer cultures cardiac muscle cells is a new, promising and controlled experimental model that will be helpful for further study on the cellular fundamental aspects of cardiac fibrillation and defibrillation, specially for the investigation of the nonlinear inherent mechanisms in the fibrillation phenomena. A next interesting study would be to perform a mathematical modeling of the cardiac cell activities using experimental data from the MEA.

References

Agladze K.I., Keener J.P., Müller S.C. & Panfilov A.V. [1994] ”Rotating spiral waves created by geometry”, *Science. 264, 1746-1748.*

Allessie M.A., Bonke F.I.M. & Schopman F.J.G. [1973] ”Circus movement in rabbit atrial muscle as a mechanism of tachycardia”, *Circ. Res. 33, 54-62.*

Athias P. & Grynberg A. [1987] ”Electrophysiological studies on heart cells in culture”, *The heart cells in culture. (ed. Pinson A) 125-158.*

Athias P., Vandroux D., Tissier C. & Rochette L. [2006] ”Development of cardiac physiopathological models from cultured cardiomyocytes”, *Ann. Cardiol. Angeiol. 55(2), 90-99.*

Athias P., Jacquir S., Tissier C., Vandroux D., Binczak S., Bilbault J.M. & Rossé M.[2007] ”Excitation spread in cardiac myocyte cultures using paired microelectrode and microelectrode array recordings”, *Journal of Molecular and Cellular Cardiology. 42, S3.*

Athias P., Jacquir S., Laurent G., Vandroux D., Binczak S. & Bilbault J.M.[2009] ”In vitro simulation of spiral waves in cardiomyocyte networks using multi-electrode array technology”, *European Journal of Heart Failure Supplements. 8(963).*

Banach K., Halbach M.D., Hu P., Hescheler J. & Egert U.[2003] ”Develpement of electrical activity in cardiac myocyte aggregates derived from mouse embryonic stem cells”, *Am. J. Physiol. Heart Circ. Physiol. 284,H2114-23.*

Beuter A., Glass L., Mackey M.C. & Titcombe M.S.[2003] ”Nonlinear Dynamics in Physiology and Medecine”, *Mathematical Biology, Springer.*

Davidenko J.M., kent P.F., Chialvo D.R., Michaels D.C. and Jalife J. [1990] ”Sustained vortex-like waves in normal isolated ventricular muscle”, *Proc. Natl. Acad. Sci. U.S.A. 87, 8785-8789.*

Davidenko J.M., Pertsov A.M., Salomonsz R., Baxter W. & Jalife J. [1992] ”Stationary and drifting spiral waves of excitation in isolated cardiac muscle”, *Nature. 335, 349-351.*

Everett T.H., Wilson E.E., Verheule S., Guerra J.M., Foreman S. & Olgin J.E. [2006] ”Structural atrial remodeling alters the substrate and spatiotemporal organization of atrial fibrillation: a comparison in canine models of structural and electrical atrial remodeling”, *Am. J. Physiol. Heart Circ. Physiol. 291, 2911-2923.*

Fast V.G. & Kleber A.G. [1995] ”Cardiac tissue geometry as a determinant of unidirectional conduction block: assessment of microscopic excitation spread by optical mapping in patterned cell cultures and in a computer model”, *Cardiovascular Research. 29, 697-707.*

Garfinkel A., Chen P.S., Walter D.O., Karagueusian H.S., Kogan B., Ewans S.J., Karpoukhin M., Hwang C., Uchida T., Gotoh M., Nwasokwa O., Sager P. & Weiss J.N. [1997] "Quasiperiodicity and Chaos in Cardiac Fibrillation", *The Journal of Clinical Investigation. 99(2), 305-314.*

Gray R.A., Jalife J., Panfilov A.V., Baxter W.T., Cabo C., Davidenko J.M. & Pertsov A.M. [1995] "Mechanisms of cardiac fibrillation", *Science. 270, 1222-1223.*

Gray R.A., Pertsov A.M. & Jalife J. [1997] "Spatial and temporal organization during cardiac fibrillation", *Nature. 392, 75-78.*

Grynberg A.[1986] "Primary rat cardiac cell culture: diet of the mother rats as a determinant parameter of cardiomyoblast production from neonates", *Biol. Cell. 57, 89-92.*

Hescheler J., Halbach M., Egert U., Lu Z.J., Bohlen H., Fleischmann B.K. & Reppel M.[2004] "Determination of electrical properties of ES cell-derived cardiomyocytes using MEAs", *J. Electrocardiol. 37, 110-116.*

Jacquir S., Tissier C., Vandroux D., Binczak S., Bilbault J.M., Rossé M. & Athias P.[2008] "Paired microelectrodes and microelectrode array analysis of cardiac impulse propagation in cardiomyocyte cultures", *Fundamental Clinical Pharmacology. 22(1), 51-52.*

Jacquir S., Laurent G., Vandroux D., Binczak S., Bilbault J.M. & Athias P.[2009] "In vitro simulation of spiral waves in cardiomyocyte networks using multi-electrode array technology", *Archives of Cardiovascular Diseases. 102(1), S63.*

Jacquir S., Laurent G., Vandroux D., Binczak S., Bilbault J.M. & Athias P.[2009] "In vitro simulation of spiral waves in cardiomyocyte networks using multi-electrode array technology", *Fundamental Clinical Pharmacology. 23(1), 68.*

Jacquir S., Xu B., Bakir T., Bilbault J.M. & Binczak S.[2009] "Analysis of Cardiac Cells Field Potentials using Wavelet Transform", *36th International Conference IEEE on Computers in Cardiology, IEEE Proceedings (ISSN 0276-6574). 36, 401-404.*

Jalife J. [2003], *J. Cardiovasc. Electrophysiol. 14(7),776-780.*

Kondratyev A.A., Ponard J.G.C., Munteanu A., Rohr S. & Kucera J.P.[2007] "Dynamic changes of cardiac conduction during rapid pacing", *American Journal Of Physiology Heart And Circulatory Physiology. 292, H1796-H1811.*

Koura T., Hara M., Takeuchi S., Ota K., Okada Y., Miyoshi S., Watanabe A., Shiraiwa K., Mitamura H., Kodama I. & Ogawa S. [2002] "Longitudinal to Transverse With Increasing Age Optical Mapping: Preferential Direction of Conduction Block Changes From Anisotropic Conduction Properties in Canine Atria Analyzed by High-Resolution", *Circulation. 105, 2092-2098.*

Laurent G., Moe G.W., Hu X., Pui-Sze So P., Ramadeen A., Leong-Poi H., Doumanovskaia L., Konig A., Trogadis J., Courtman D., Strauss B.H. & Dorian P. [2008] "Simultaneous right atrioventricular pacing: a novel model to study atrial remodeling and fibrillation in the setting of heart failure", *J. Card. Fail. 14(3), 254-262.*

Laurent G., Moe G., Hu X., Leong-Poi H., Connelly K.A., So P.P., Ramadeen A., Doumanovskaia L., Konig A., Trogadis J., Courtman D., Strauss B. & Dorian P.[2008] "Experimental studies of atrial fibrillation: a comparison of two pacing models", *Am. J. Physiol. Heart Circ. Physiol. 294(3), H1206-15.*

Laurent G., Jacquir S., Binczak S., Vandroux D., Bouchot O., Wolf J.E., Athias P. & Bilbault J.M.[2008] "Establishing a novel in vitro model for the study of spiral waves during arrhythmia", *European Heart Journal. 29(166).*

Lim Z.Y., Maskara B., Aguel F., Emokpae R. & Tung L.[2006] "Spiral Wave Attachment to Millimeter-Sized Obstacles", *Circulation. 114, 2113-2121.*

Moe G.K., Rheinboldt W.C. & bildskov J.A.[1964] "A computer model of AF", *Am Heart J. 67, 200-220.*

Panfilov A.V. and Pertsov A.M.[2001] "Ventricular fibrillation: evolution of the multiple wavelet hypothesis", *Phil. Trans. R. Soc. Lond. A 359, 1315-1325.*

Pertsov A.M., Davidenko J.M., Salomonsz R., Baxter W. & Jalife J. [1993] "Spiral waves of excitation underlie reentrant activity in isolated cardiac muscle", *Circ. Res. 72, 631-650.*

Pillekamp F., Reppel M., Brockmeier K. & Hescheler J.[2006] "Impulse propagation in late-stage embryonic and neonatal murine ventricular slices", *J. Electrocardiol. 39:425, e421-424.*

Rohr S.[2004] "Role of gap junctions in the propagation of the cardiac action potential", *Cardiovasc. Res. 62, 309-322.*

Ruelle D. & Takens F. [1971] "On the nature of turbulence", *Comm. Math. Phys. 20:167-192.*

Stett A., Egert U., Guenther E., Hofmann F., Meyer T., Nisch W. & Haemmerle H.[2003] "Biological application of microelectrode arrays in drug discovery and basic research", *Anal. Bioanal. Chem. 377,486-495.*

Tissier C., Bes S., Vandroux D., Fantini E., Rochette L., Athias P.[2002] "Specific electromechanical responses of cardiomyocytes to individual and combined components of ischemia", *Can. J. Physiol. Pharmacol. 80, 1145-1157.*

Wang T.J., Larson M.G., Levy D., Vasan R.S., Leip E.P., Wolf P.A., D'Agostino R.B., Murabito J.M., Kannel W.B. & Benjamin E.J. [2003] "Temporal relations of atrial fibrillation and congestive heart failure and their joint influence on mortality: The Framingham Heart Study", *Circulation. 107, 2920-2925.*

Winfree A.T. [1994] ”Electrical turbulence in 3-dimensional heart muscle”, *Science. 266, 1003-1006.*

Fig. 1. Cardiac myocyte of new born rat [Athias et al, 2006]. The blue color shows the nucleus and the red color shows the contractile sarcomeric apparatus.

Fig. 2. MEA dish with cardiac cells of newborn rats. (a) is a global view of the MEA dish, (b) is a microscopic view of the microelectrodes matrix (magn. $10X$), (c) is a microscopic view of the cardiomyocyte monolayer grown on the microelectrodes matrix (magn. 40X).

Fig. 3. Setup allowing field potential recordings from cardiac muscle cells in monolayer culture. A: Amplification device, B: Faraday enclosure, C: Temperature regulator, D: Acquisition and data processing platform.

Fig. 4. (a) Field potential time series in the basal conditions (correct signal in blue, rejected signals in red). (b) Example of the field potential serie corresponding to one microelectrode. The FP period or frequency is computed between two successive spikes. The appearance of the successive FP spike vs. time gives the local activation time (LAT). Abscissa: Time (s). Ordinate: Amplitude (V) of the FP.

Fig. 5. Distribution of the mean periods of the field potentials (FP) train corresponding to data presented in Fig. 4(a) with the standard deviation. The inaccurate signals are excluded of the calculus.

Fig. 6. Local activation maps of the field potentials. The white arrow indicates the direction of FP propagation. Panel (a) corresponds to the appearance of the first FP, while the panel (h) corresponds to the appearance of the eightth FP. *NaN* indicates the rejected inaccurate signals.

Fig. 7. Bifurcation diagram of the field potential periods P for the time series given by the 60 microelectrodes. The microelectrode $M1$ (see Fig. 2(a)) is used to stimulate electrically the cells in culture during 5 min with a burst of 200 μV of amplitude and 100 Hz of frequency. The cells behavior during time exhibits special features : (A) (at $t = 1$ hour after stimulation) corresponds to a chaotic state, (B) (at 3 hours after stimulation) corresponds to a period doubling phase, (C) (at $t = 4$ hours after stimulation) corresponds to a regular and stable rhythm.

Fig. 8. Poincaré map of the FP periods ($P_{n+1} = f(P_n)$) in basal conditions (data presented in Fig. 4(a)).

Fig. 9. Example of field potentials in a chaotic phase (event (A) in the bifurcation diagram (Fig. 7)). Panel (a) shows field potential time series (correct signal in blue, rejected signals in red). Abscissa: Time (s). Ordinate: Amplitude (V) of the FP. Panel (b) shows a Poincaré map of the FP periods ($P_{n+1} = f(P_n)$).

Fig. 10. Example of field potentials in a period doubling phase (event (B) in the bifurcation diagram (Fig. 7)) . Panel (a) shows field potential time series (correct signal in blue, rejected signals in red). Abscissa: Time (s). Ordinate: Amplitude (V) of the FP. Panel (b) shows a Poincaré map of the FP periods ($P_{n+1} = f(P_n)$).

Fig. 11. Example of field potentials in a stable rhythm phase (event (C) in the bifurcation diagram (Fig. 7)). Panel (a) shows field potential time series (correct signal in blue, rejected signals in red).

Abscissa: Time (s). Ordinate: Amplitude (V) of the FP. Panel (b) shows a Poincaré map of the FP periods ($P_{n+1} = f(P_n)$).

Fig. 12. Visualization of a relatively stable counter-rotating spiral wave during a sustained induced arrhythmia episode induced by external electrical stimulation (the letters ($(a) \longrightarrow (b) \longrightarrow (c) \longrightarrow (d) \longrightarrow (e) \longrightarrow (f)$) indicate the clockwise rotation). Experimental data were smoothed using a cubic spline interpolation. The first image (item (a) corresponding to time 0.482 s) shows the initiation and the last image (item (f) corresponding to time 0.676 s) illustrates the termination of the SW. The red color indicates the depolarization of cells and the blue color indicates the refractory period. The size of each panel corresponds to the recording area surface (2.5 mm^2).

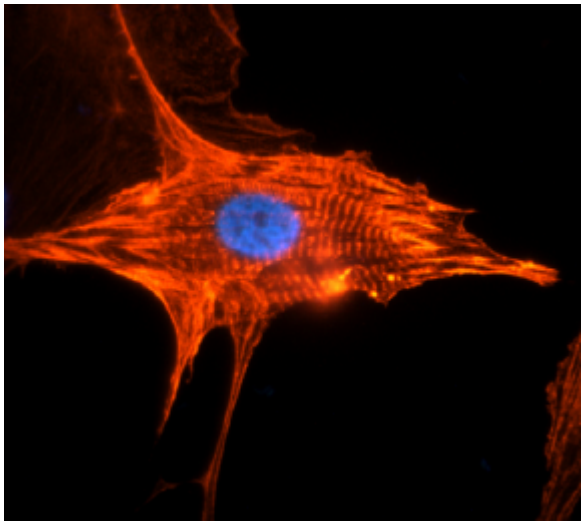

Figure 1:

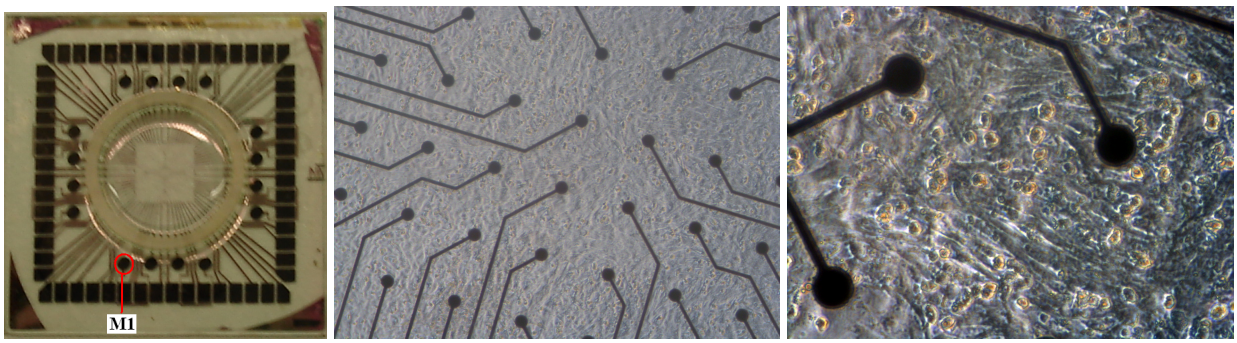

(a) (b) (c)

Figure 2:

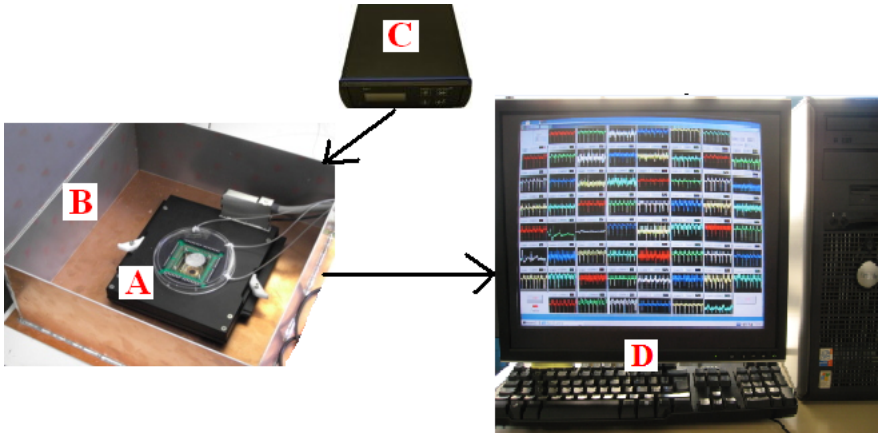

Figure 3:

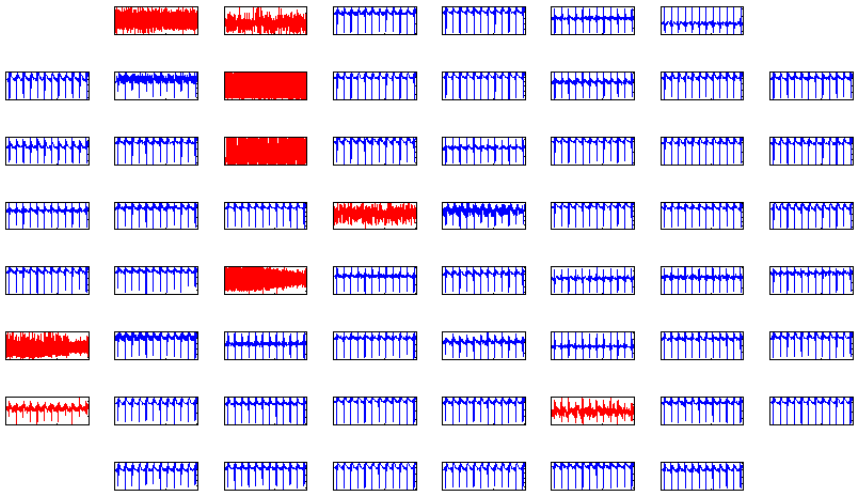

(a)

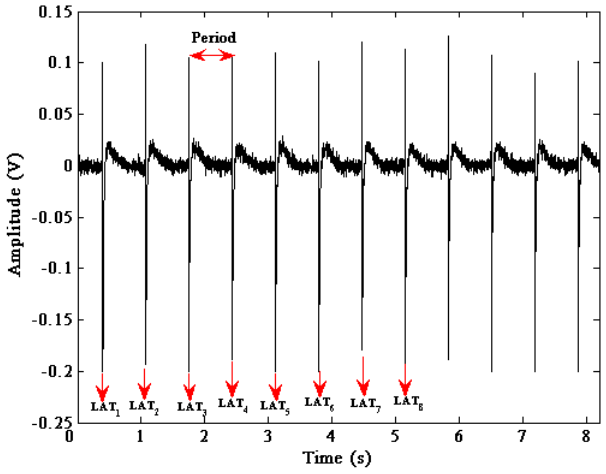
Period
Amplitude (V)
Time (s)
0.15
0.1
0.05
0
-0.05
-0.1
-0.15
-0.2
-0.25
0
1
2
3
4
5
6
7
8
LAT1
LAT2
LAT3
LAT4
LAT5
LAT6
LAT7
LAT8

(b)

Figure 4:

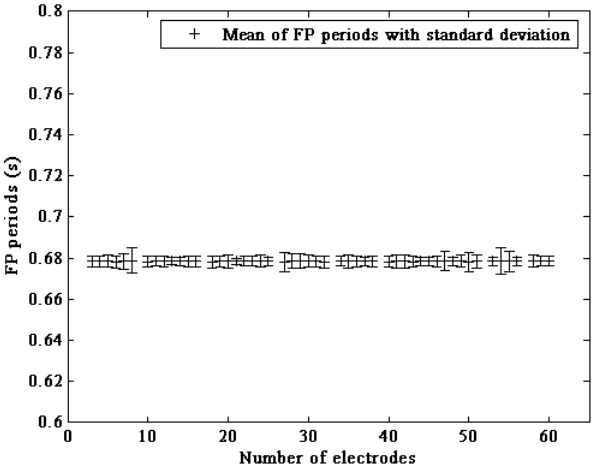
Mean of FP periods with standard deviation
FP periods (s)
Number of electrodes
0.8
0.78
0.76
0.74
0.72
0.7
0.68
0.66
0.64
0.62
0.6
0
10
20
30
40
50
60

Figure 5:

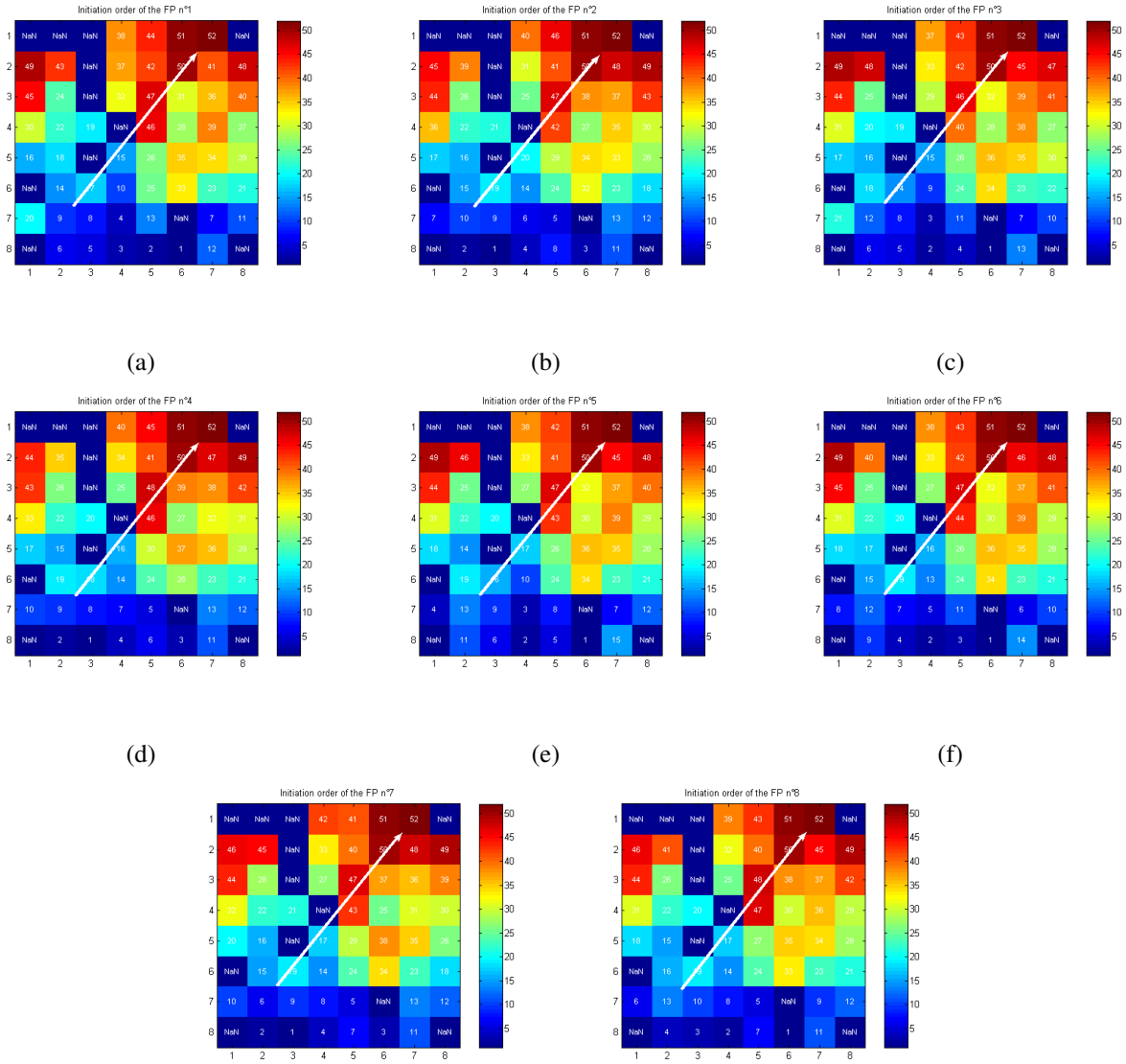
Initiation order of the FP n°1
Initiation order of the FP n°2
Initiation order of the FP n°3
(a)
(b)
(c)
Initiation order of the FP n°4
Initiation order of the FP n°5
Initiation order of the FP n°6
(d)
(e)
(f)
Initiation order of the FP n°7
Initiation order of the FP n°8
(g)
(h)

Figure 6:

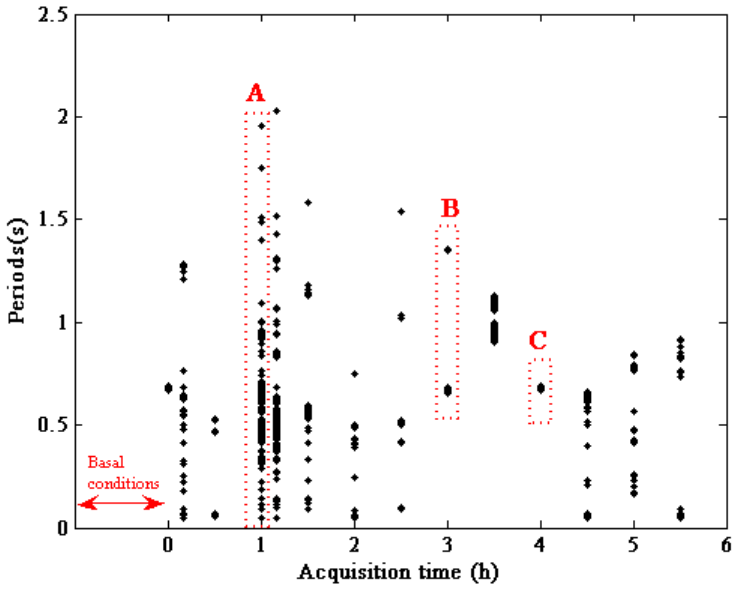
A
B
C
Basal
conditions
Periods(s)
Acquisition time (h)
0
0.5
1
1.5
2
2.5
0
1
2
3
4
5
6

Figure 7:

Figure 8:

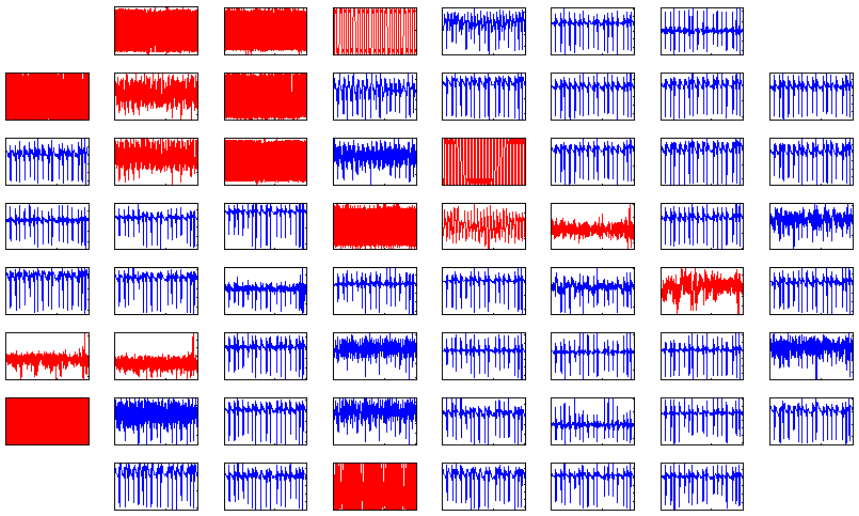

(a)

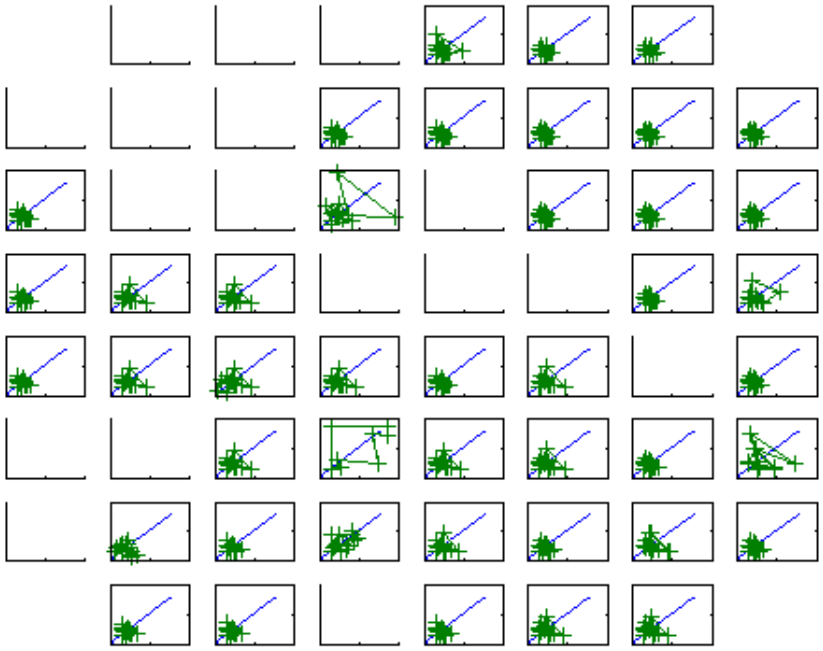

(b)

Figure 9:

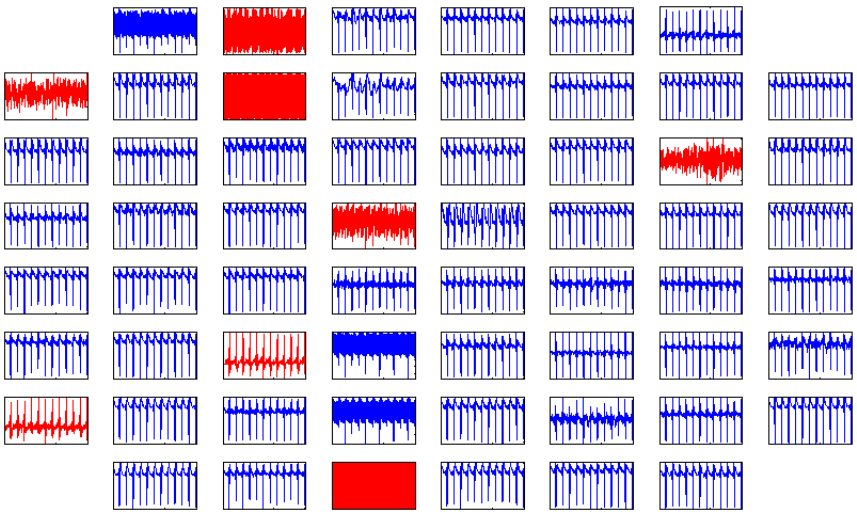

(a)

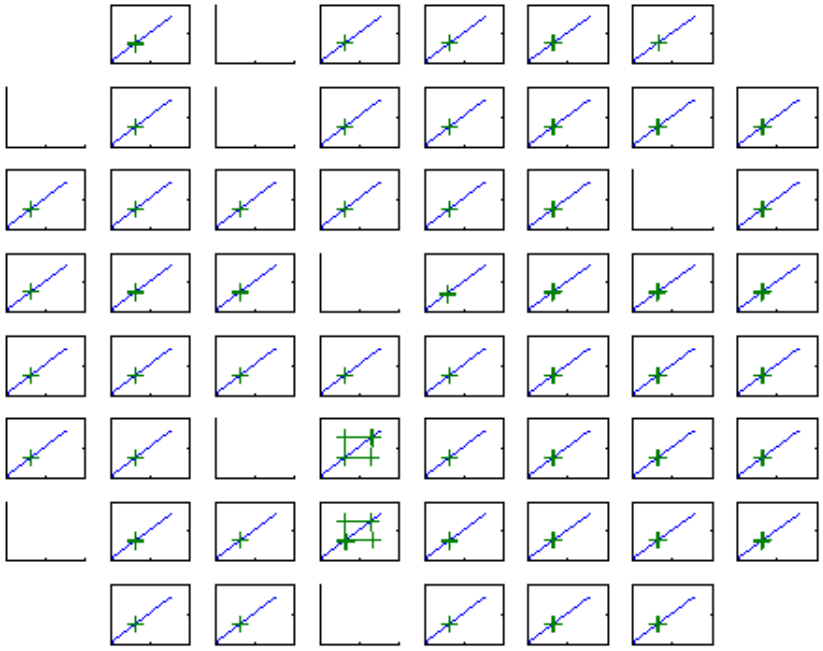

(b)

Figure 10:

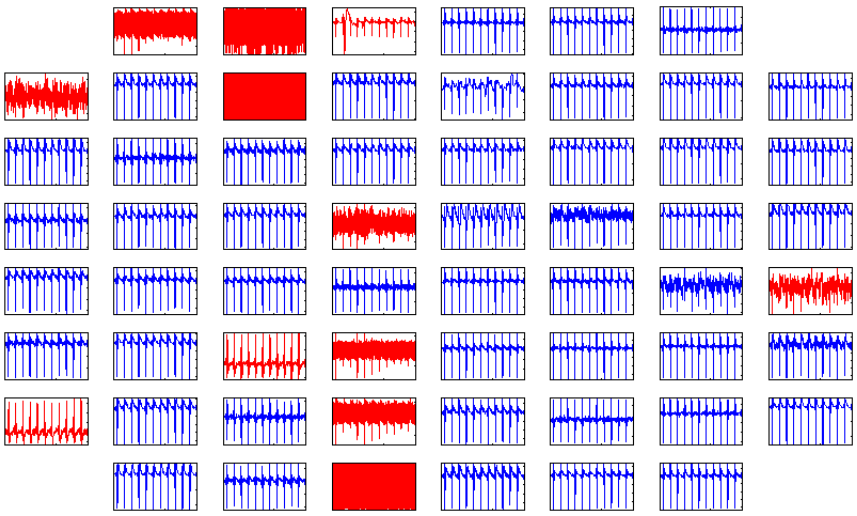

(a)

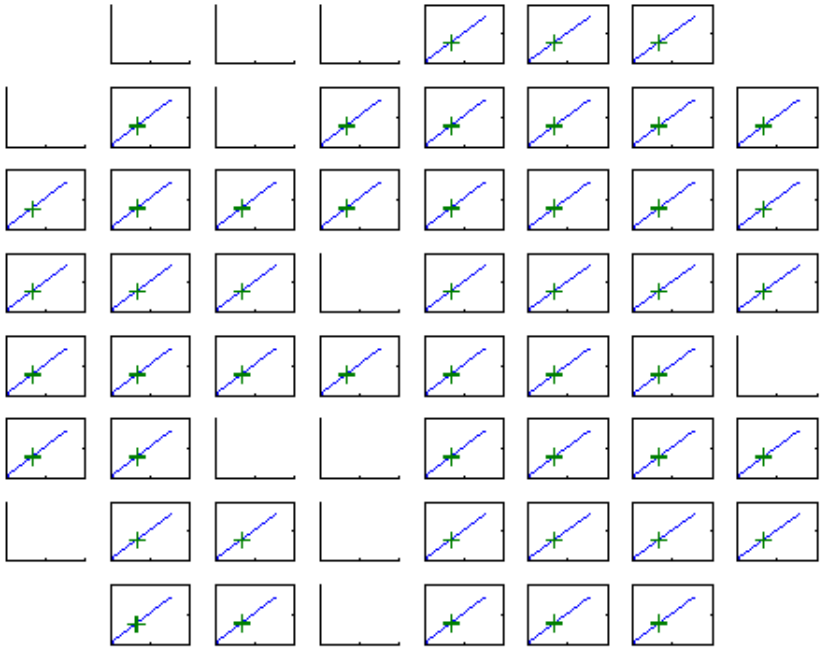

(b)

Figure 11:

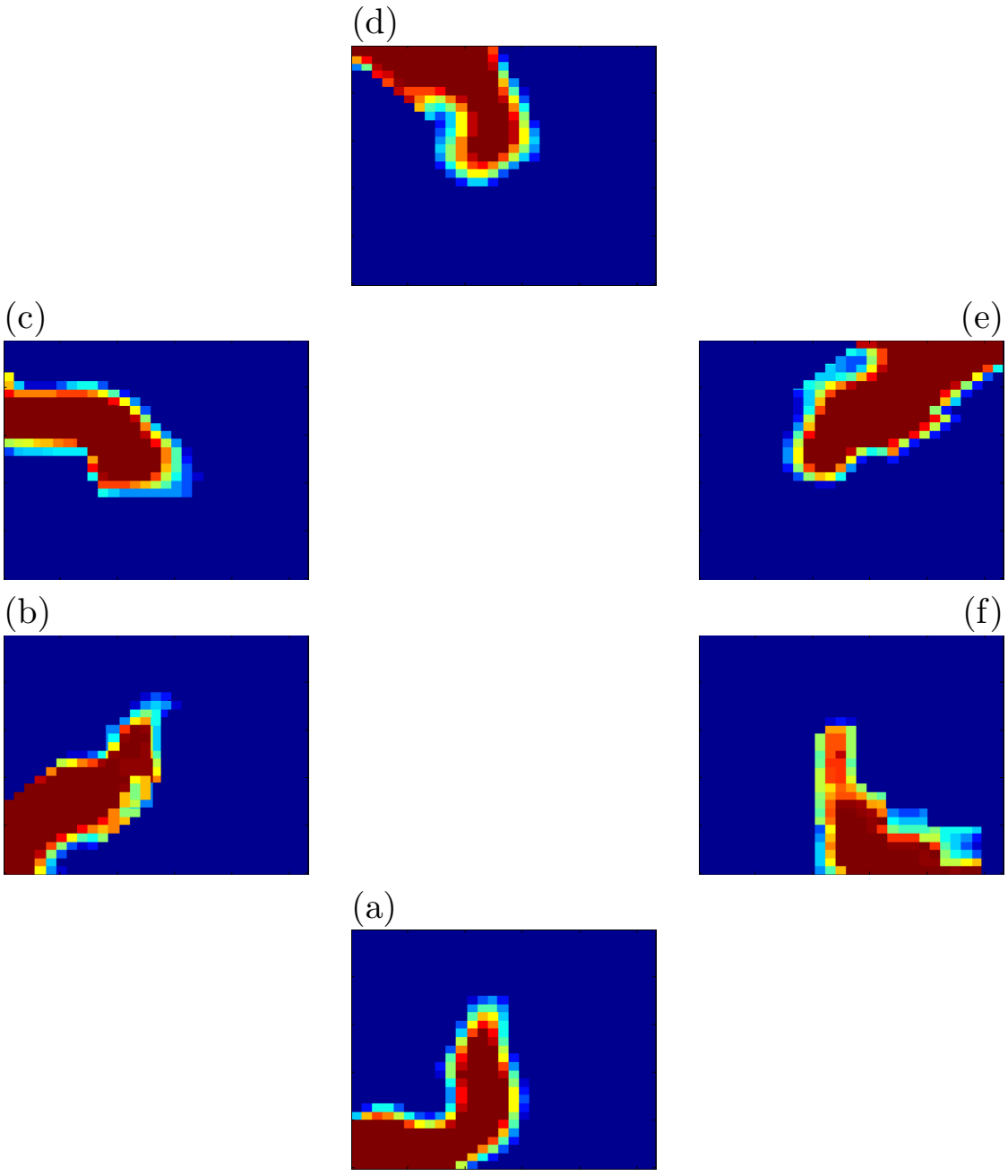

Figure 12: